

CHAPTER 2

Pointing and Gain Calibration of the 10.4m Telescope

2.1 A brief description of the telescope system

The site:

The 10.4 m millimeter-wave telescope at the Raman Research Institute in Bangalore, is a Cassegrain type antenna on an altitude-azimuth mount, with the receiver at the Nasmyth focus. This telescope is located on campus, at the latitude = $13^{\circ} 01'$, longitude = $77^{\circ} 35'$, and at an elevation of 930 meters above mean sea level. This site is driest during November to March, with a median value of precipitable water of about 15mm (Maiyah, 1983). This period of the year is therefore the usual observing season with a zenith optical depth of about 0.15 at a frequency of 86 GHz. During the rest, of the year, the precipitable water vapour exceeds 20–25mm and the zenith optical depth is usually greater than 0.6.

The system:

The Telescope's control system consists of DC motors (2 motors per axis, with a differential torque to avoid 'backlash' errors in the gears), and 21 bit Inductosyn type encoders. A PDP 11/84 computer reads a digital clock and the encoders every 0.1 seconds and computes the desired azimuth and elevation, given the RA and Dec of the source. A velocity servo program then drives the motors to track the source. During the observing season the wind speed is usually less than 5 km/sec, rarely reaching 10 to 15 km/sec, and therefore does not offer any problem in tracking.

A schematic diagram of the telescope optics is given in Figs 1 and 2. The primary is a 10.4 meter diameter paraboloid constructed from hexagonal panels (pre-cut in a paraboloidal shape and re-assembled on site). The design and con-

structional details are as given by Leighton (1978). Except the mount, the entire telescope system was constructed at Bangalore, following Leighton's design with a modification only in the elevation drive. The mount was fabricated by a commercial firm in Bombay. The secondary is a hyperboloid of diameter 60cms and eccentricity 1.06; made from aluminium with a numerically controlled machine and with a surface error of only a few microns. It is movable by a motor, along the optical axis, for adjusting the focus. The tertiary is an aluminium plate acting as a flat mirror, that can be rotated about an axis perpendicular to the elevation axis, to enable beam-switching in azimuth. The ray diagram for the beam-switching signal is shown in Fig. 2. The radiation after reflection from the tertiary, enters the elevation axis tube and goes through a grooved teflon plano-convex lens of focal length of 27cm and diameter of 13cm. The radiation is coupled by this lens to a quasi-optical diplexer which is closely attached to the dewar containing the mixer and pre-amplifier both cooled to about 20K. The local oscillator is a gunn oscillator tunable between 85 to 120 GHz. The block diagram of the receiver system is shown in Fig. 3.

The back-end consists of a synchronous-detector for continuum measurements and the following spectrometers.

Table 1. Spectrometers

Filter Banks		
No. of channels	Resolution (frequency)	Velocity width (km/sec 86GHz)
256 ¹	250 Khz	0.87
64	1 Mhz	3.48
128	50 Khz	0.17

¹Used for SiO observations reported in this thesis.

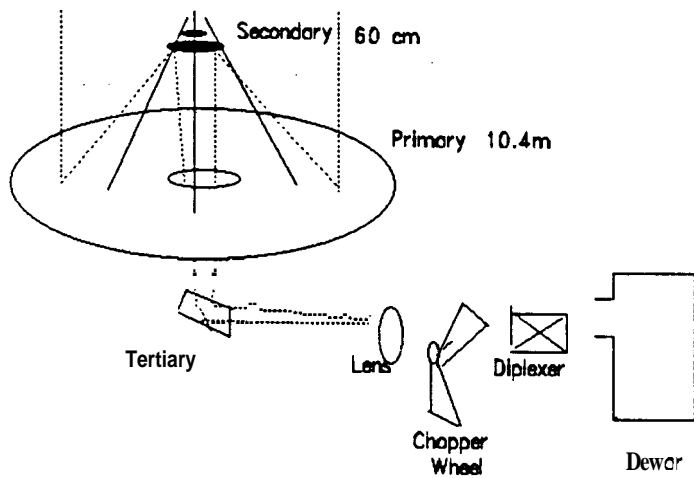


Figure 1: Schematic of the 10.4M Telescope Optics

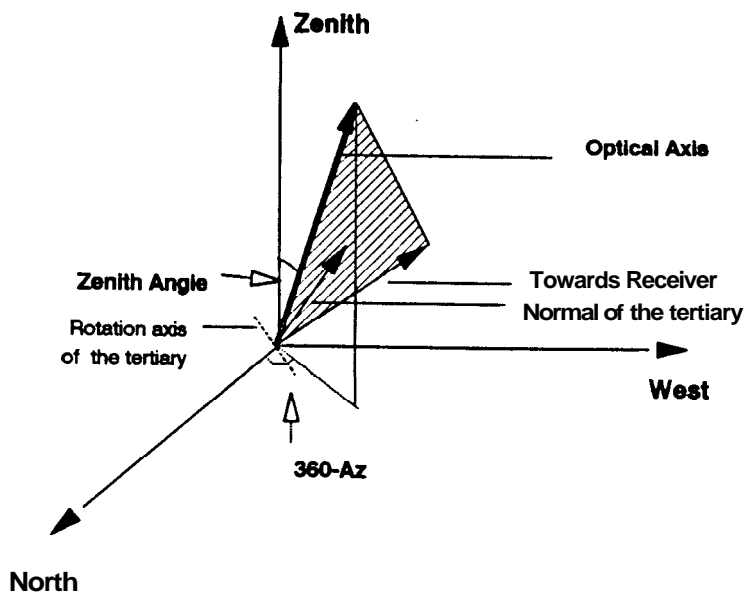


Figure 2: Ray diagram for the beam-switching system

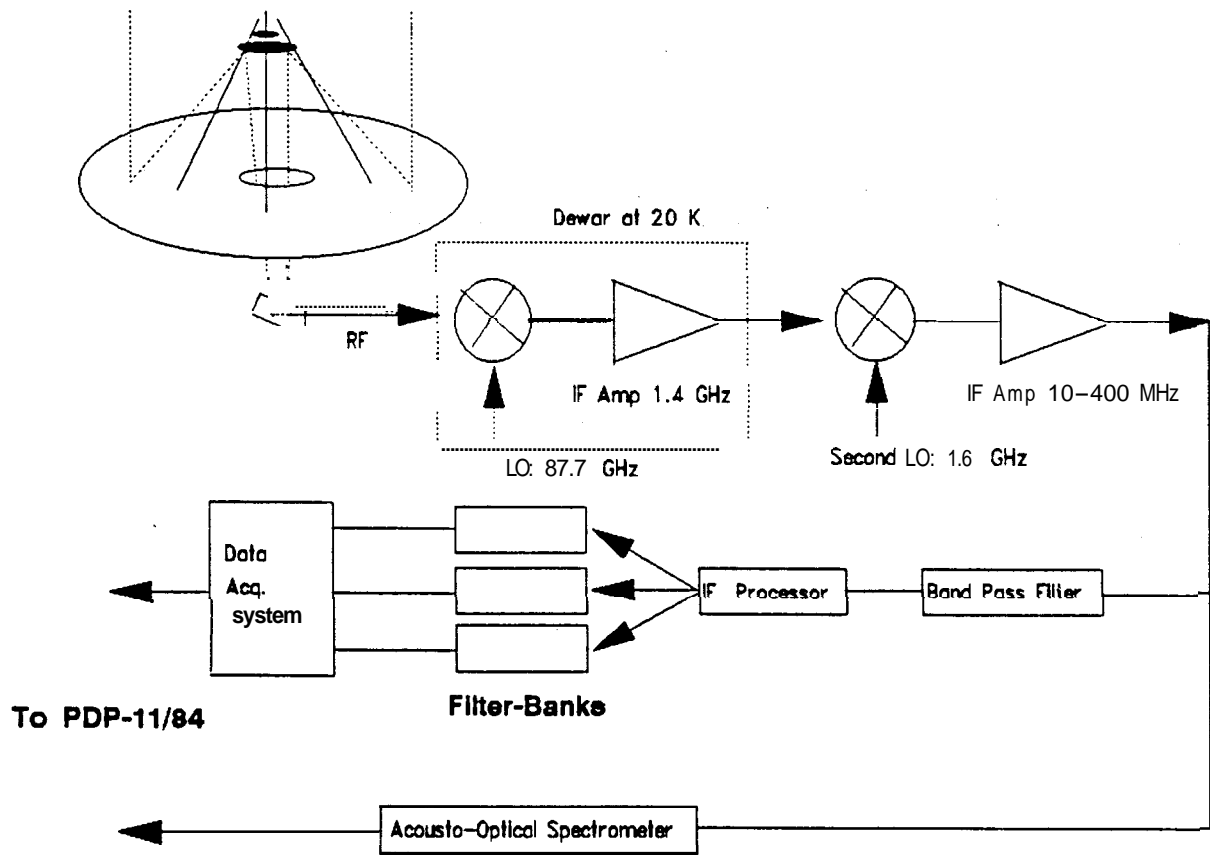


Figure 3: Block diagram of the receiver system

Acousto-optical spectrometers

Total bandwidth	Effective resolution (frequency)	Velocity width (km/sec 86GHz)
120 ¹ MHz	210 KHz	0.73
40 MHz	66 KHz	0.23
400 MHz	1 MHz	3.48

The 256 channel filter-bank and the 40 MHz AOS are read by a M68000 microprocessor based data acquisition system which communicates the data to the PDP 11/84 roughly every 10 minutes. The PDP 11/84 reads the 120 MHz AOS separately.

The typical values of system temperatures at zenith, for the three seasons during which the observations reported in this thesis were made, are given in the following Table.

Table 2. Typical values of System Temperature

Year	$T_{\text{sys}}(\text{zenith})$ (DSB)
1988	456 K
1989	406 K
1990	523 K

The zenith optical depth was frequently monitored by taking Dip scans on the sky. Typical scans on a clear sky and cloudy sky are shown in Fig. 4.

The observations were calibrated using a chopper-wheel positioned between the diplexer and the lens.

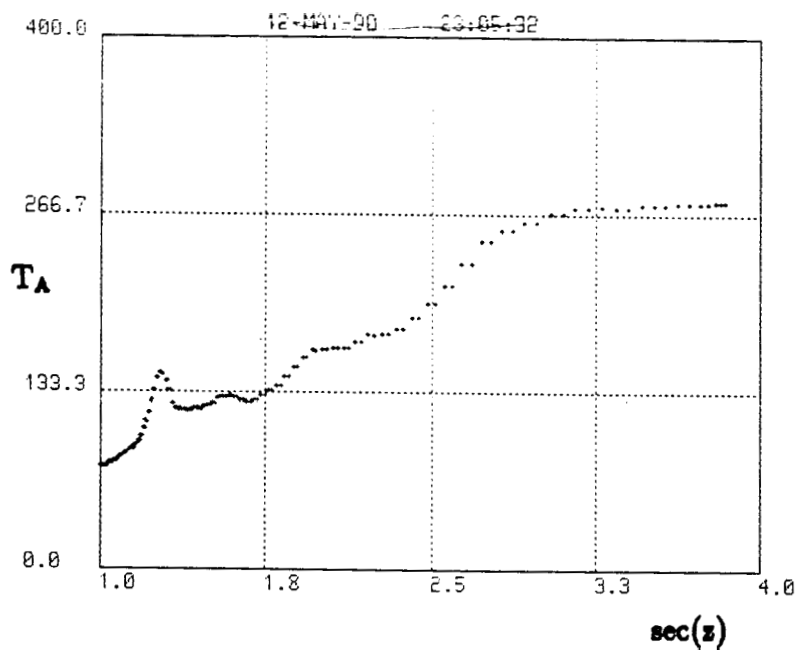
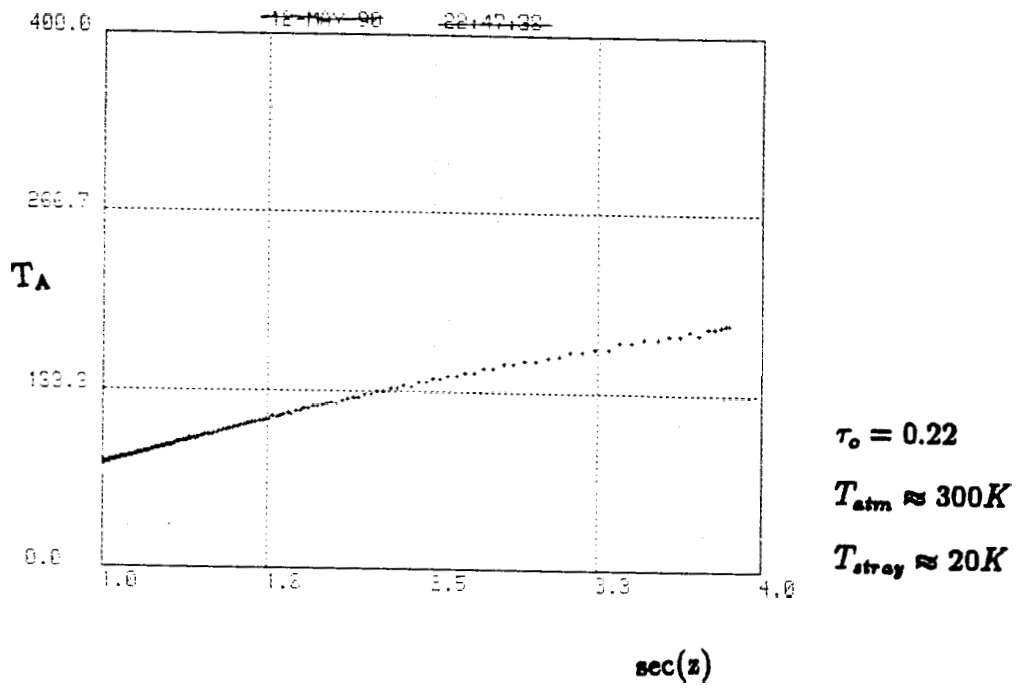


Figure 4: Atmosphere's optical depth as a function of $\sec(z)$ on a clear sky (above), and on a cloudy sky (below).

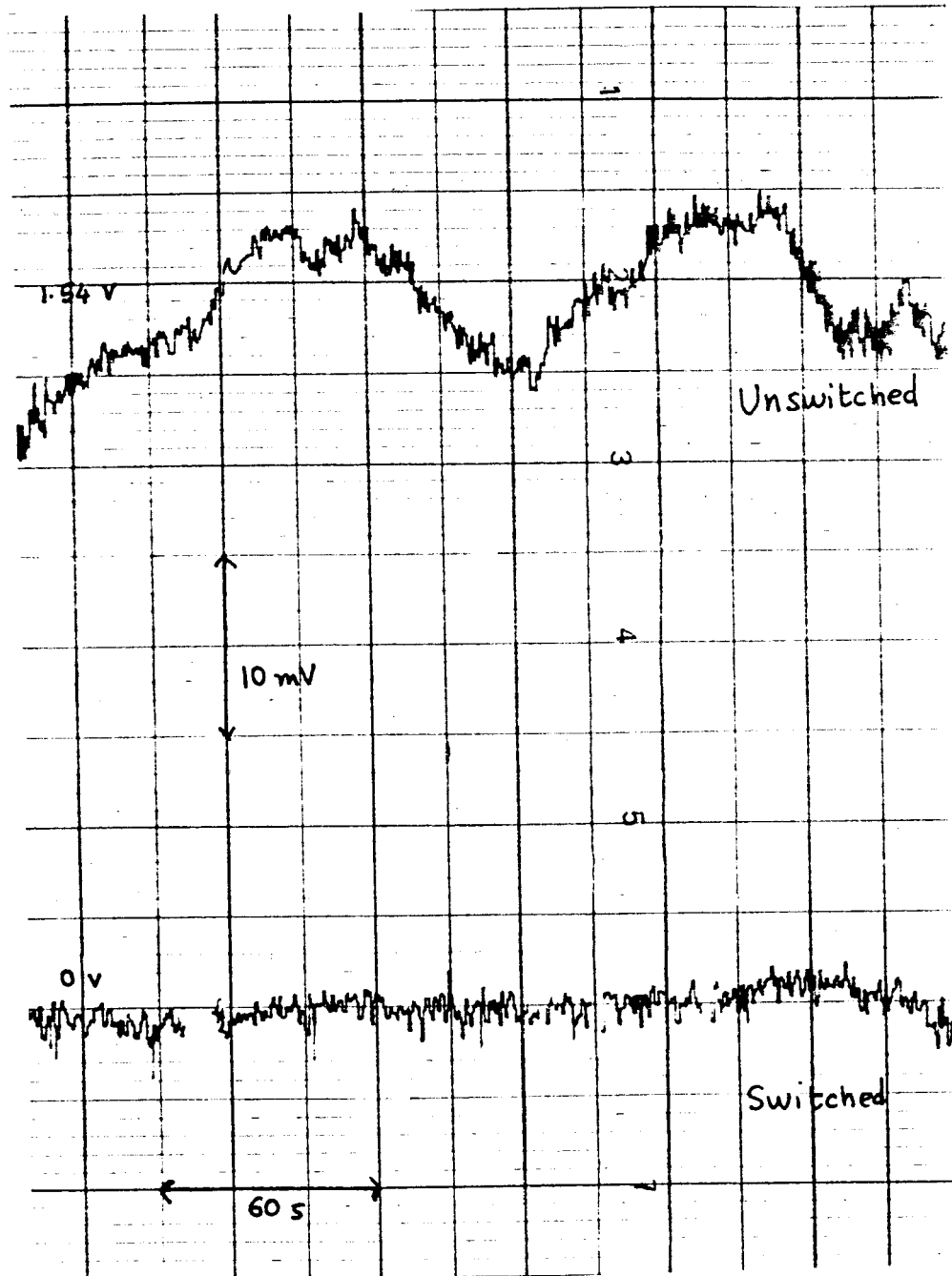


Figure 5: Plot of total-power voltage ("Unswitched"), and the synchronous-detector voltage ("Switched"), as a function of time.

2.2 Beam Switching

A typical radio astronomical measurement involves the detection of a very weak signal against a background of a much stronger signal partly from the instrument itself and partly from the sky. For example, the antenna temperature measured on say Jupiter may be of the order of 10K while the system temperature is around 450K; moreover, spectral-line observations of say SiO maser sources give antenna temperatures that are typically much less than 10K and the system temperature is now about 900K (SSB). Not only is this background noise much larger in magnitude than the signal that one is trying to measure, but it also varies in time, often on a scale of seconds due to variations in gain, atmospheric attenuation etc. Hence the need for switching i.e., a rapid comparison of the signal from the source with that from the 'background'. There are various well-known schemes to achieve this (Williams 1976).

Fig. 5 is a plot of the total-power voltage as a function of time, corresponding to the power integrated over a bandwidth of 400 MHz with the telescope pointed at the sky. This quantity is labelled "Unswitched". In the same figure, the synchronous detector output voltage at a switching rate of 2 Hz, is labelled "Switched". The variations in the total-power voltage mainly reflect the inhomogeneities in the atmosphere which are moving. The variations due to the gain of the receiver are much slower. Thus, for an observation of a source in a given direction, one needs to compare it with one in a neighbouring direction which is close enough to ensure the same emission from the sky but far enough to clear the source itself to avoid cancelling its signal. Also, the switching should be fast enough to cancel the variation of the sky emission. This can be done by steering the telescope itself (position switching), but it has limitations on the speed

at which one can switch this way. It takes about 20 seconds for our telescope to reach an 'off-source' position. Position switching at a faster rate and with smaller angle is referred to as 'Beam Switching' and is usually achieved without moving the telescope. In a prime focus system, to change the direction of the beam on the sky by an angle θ , the feed has to be displaced in the focal plane by an amount $\epsilon = F\theta$, where F is the focal length of the primary paraboloid. This shift can be achieved by either moving the feed itself mechanically, or by moving its virtual image, as seen by the secondary, by rotating the tertiary mirror. For small ϵ , the phase error in the illumination across the primary in the direction of this shift is a linear function of the perpendicular distance from the optical axis, giving rise to a steered beam. As ϵ increases, a cubic term in the phase error becomes significant, resulting in coma aberration. In units of beamwidths, n , the limiting value of beam throw beyond which coma aberration enters, is given by Christiansen and Hogbom (1969).

$$0.075n = (F/D)^2. \quad (1)$$

For the 10.4m telescope, the F/D ratio is 0.38, therefore one can change the direction of the beam by about twice the beam size without a coma. Further, since the secondary's eccentricity is 1.06, the equivalent displacement at the (Nasmyth) focal plane corresponding to this limiting beam throw is about 11 cm.

In most telescopes, one tilts or nutates the secondary for beam-switching. The disadvantages lie in the fact that the hardware for moving the secondary is often bulky and it is undesirable to have a weight at the prime focus because it may increase the sag of the quadripod leading to beam-distortion in the plane containing the zenith and the optical axis and decreasing with the elevation. Secondly, when the secondary tilts in order to steer the beam on the sky after

reflection from the primary, some part of the feed's response misses the primary and may terminate on the ground, increasing the system temperature. At the 10.4m telescope, the beam switching is done by a rotating tertiary mirror. Since we believe that this system is a novel one, it is discussed in detail below. The inconvenience of having a mechanical load at the prime focus is avoided by using the tertiary for beam switching. The 'off' beam terminates on the sky leading to a less significant increase in the system temperature. Moreover, the direction of the beam throw is in the same sense as the motion of the tertiary, so the spillover past the secondary in the 'off' beam is in the same region of the sky which is seen by the main beam and at the same elevation. However, it should be noted that the spilled over beam has an angular size corresponding to the size of the feed and hence much larger than the main beam. The amount of beam throw on the sky as a result, of rotation of the mirror by a small angle away from 45° is derived as follows. One can think of the rotating tertiary as shifting the virtual image of the feed at the Nasmyth focal plane, as seen by the secondary. This is shown in Fig. 6.

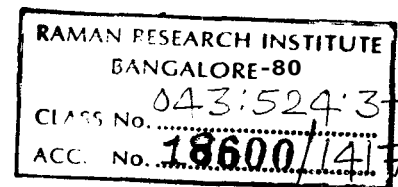
The shift in this virtual image is given by

$$\epsilon = D \times \tan(2\theta_m), \quad (2)$$

Where θ_m is the angle of rotation of the mirror from its 45° position. Thus, the beam throw is given by

$$\theta_T = \frac{\epsilon}{MF} \approx 3000'' \tan(2\theta_m), \quad (3)$$

where $M = \frac{\epsilon+1}{\epsilon-1}$.



Mechanical Aspects:

The mirror is rotated by a stepper-motor through a link as shown in the Fig. 7. The switching positions correspond to the steps of the motor. These positions of the mirror are measured by an encoder which is a metal disk on the axis of the motor used for switching and has codes marked on it radially corresponding to the steps of the motor. The codes are read by an optical sensor. The mode of switching is programmable and is controlled by the PDP computer during observation. The switching rates can be set manually to 1,2 or 4 Hz. There are two modes of switching: the first one is symmetrical about the center of the secondary, and the second between the center of the secondary and an off position which misses the secondary. In both the modes there are two ranges of amplitudes one can choose. At the motor shaft, one step corresponds to 0.0314 radians (1.8°). The link (see Fig. 7) converts this angle to 0.00338 radians around the mirror's axis. Using eqn. 3, we get Table 3, of beam throws corresponding to the various modes.

Table 3. Modes of beam-switching

Mode	Throw in Motor-steps	Beam-throw on the sky
1	+2-2	80"
2	+4-4	160"
3	0-18	$3^\circ.5$
4	0-22	$4^\circ.3$

Note that for the last two modes in the Table 3, eqn. 3 is not valid because in these two modes, the off positions miss the secondary and look at the sky directly, with a beam that is about a 100 times larger than that of the primary. (The radius of the secondary subtends an angle of $2^\circ.9$ at the tertiary).

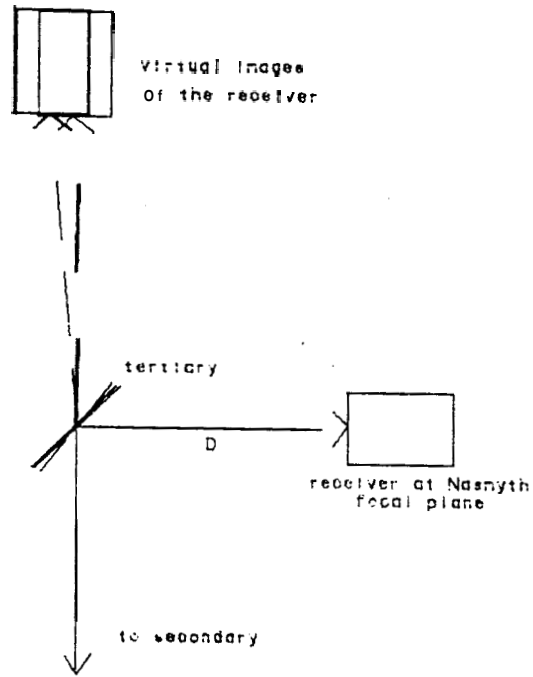


Figure 6: Shift of the virtual image by rotating the tertiary

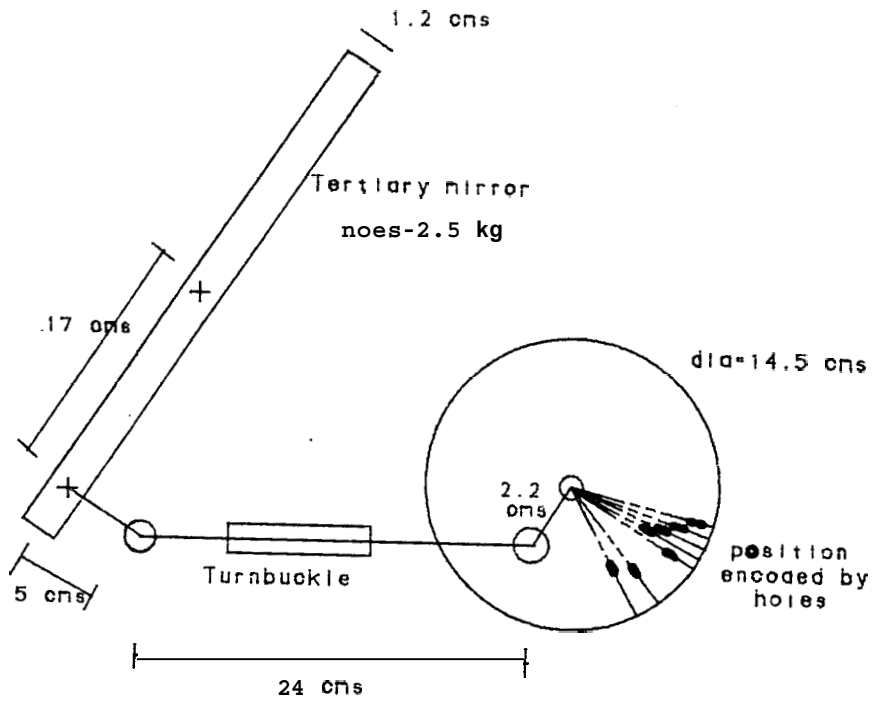


Figure 7: Beam switching mechanism

Calculation of the required torque to rotate the mirror: The velocity of travel is constant after the 1st step of the motor. Thus, with the varying rate, what changes is not the angular velocity, but only the amount of time for which the mirror stays at each end position. The angular velocity is fixed: 1 step in 3 ms. The acceleration occurs only in the 1st step during which the above uniform velocity is attained. Neglecting the mass of the link and assuming the mirror of mass 2.5 kg to be thin, the moment of inertia works out to be 305 kg cm^2 . Its angular acceleration is 188 rad s^{-2} . Thus the required torque is $57311 \text{ kg cm}^2 \text{ s}^{-2}$ (i.e. 58.48 kgcm in usual units of specification). This is the torque required at the mirror axis. Neglecting friction at all points of the machine, the torque required at the motor axis is 6.3 kgcm. To this one should add the torque required to move the rotor alone. The motor used is a Slosyn model M092 whose rotor's moment of inertia is 1.23 kgcm^2 . Therefore the total torque required is 8.49 kgcm, while the torque provided by this motor was 14.4 kgcm.

2.3 Pointing Correction

The 10.4m telescope has an altazimuth mount. Due to tilts in the azimuth and elevation axes, there can be systematic pointing errors. We refer to the source of these pointing errors as mount errors. The mount errors include: 1. Tilt in the azimuth axis with respect to the true zenith (described by an upward projection of a dropped plumb-line), characterized by two angles. 2. Tilt in the elevation axis, which measures the non-orthogonality with respect to the azimuth axis. 3. Collimation error: this is the angle made by the radio axis (the direction towards which the antenna's response is maximum) with the plane that is normal to the elevation axis. By definition, this is an error only in azimuth. The other component of the error if any, is a fixed amount of offset in elevation, just like a dc error in the elevation encoder.

Of these errors, the azimuth axis tilt is measurable easily and accurately by a pair of inclinometers mounted on the azimuth platform of the telescope. The elevation axis tilt is not measurable. The collimation error can in principle be predicted by knowing the relative tilts in the various optical components, the primary dish's tilt, the secondary's tilt and lateral offsets, the quadripod's tilts etc. These parameters are measurable to the extent of about 1mm in lateral errors and about $10''$ in tilts. The lateral offset from the proper position of the secondary was sufficiently reduced after measuring it by sighting it through an optical telescope mounted at a neighbouring building while the telescope was moved a full circle in azimuth. This error then was corrected by adjusting the tilts in the quadripod's legs. The residual tilt in the secondary, partly contributed now by the removal of lateral offsets, was minimised by several iterations on continuum scans on Jupiter. Pointing offsets were measured by

fitting gaussians to continuum scans taken on Jupiter, Venus and Saturn. Offsets were also obtained from observations of strong SiO maser sources: VY CMa, Orion and W Hya.

Since we employ beam switching in azimuth, we can use the following simple and quick method to estimate the pointing error in azimuth by observing a strong point-like source. This method relies on the fact that since the beam-throw is about half the beam size, towards the center of the beam-switched response pattern (i.e., the direction in which the antenna is looking), it has a steeper slope than at half-power points of the gaussian beam. If one makes two measurements separated in azimuth by a fixed amount that is smaller than the beam-separation and if the pointing error is also smaller than the beam-separation, we can obtain the pointing error ΔA from, (see Fig. 8),

$$\frac{I_1 - I_2}{2S} \approx \frac{I_1}{S + \Delta A}, \quad (4)$$

where I_1 and I_2 are the measured intensities at the points indicated in Fig. 8, and $2S$ is the beam-throw in switching which is usually of the order of an arc-minute.

From these offsets, a pointing model was obtained by a least-squares fit. This model uses the formulae for offsets as given by Ulich (1981); with the following differences — firstly, the least-squares fit did not include the azimuth axis tilt as it was measured by the inclinometers. Secondly, the encoder errors were not included. Thirdly, in correcting for the elevation offset due to gravitational flexure, we found that a more complicated function was needed for our telescope than the simple cosine of elevation as given in Ulich (1981).

The pointing errors due to tilts in the azimuth and elevation axes and due to collimation error ('mount errors') can be derived simply using spherical trigonometry as follows:

2.3.1 Pointing offsets due to mount errors

Notation used:

$\Delta A, \Delta E$: pointing corrections given to the encoders ('offsets').

A, E : azimuth and elevation.

A_o, E_o : zero point offsets in the encoders.

c : collimation error.

c' : elevation axis tilt.

I : azimuth axis tilt.

A_t : azimuth towards which the azimuth axis is tilted.

A, l : the true azimuth and l elevation.

Azimuthal error due to a tilt in the elevation axis

Only the vertical component of the tilt is relevant, the horizontal component is the same as a DC off set in the azimuth encoder.

From

$$\sin \Delta A = \tan l \tan c', \quad (5)$$

to first order in ΔA and c' ,

$$\Delta A = c' \tan l \quad (6)$$

For the elevation offset, ($X'Y'$ in Fig. 9) is given by,

$$\sin l = \sin(1 + \Delta E) \cos c' \quad (7)$$

thus, to first order, the elevation offset due to a tilt in the elevation axis is zero.

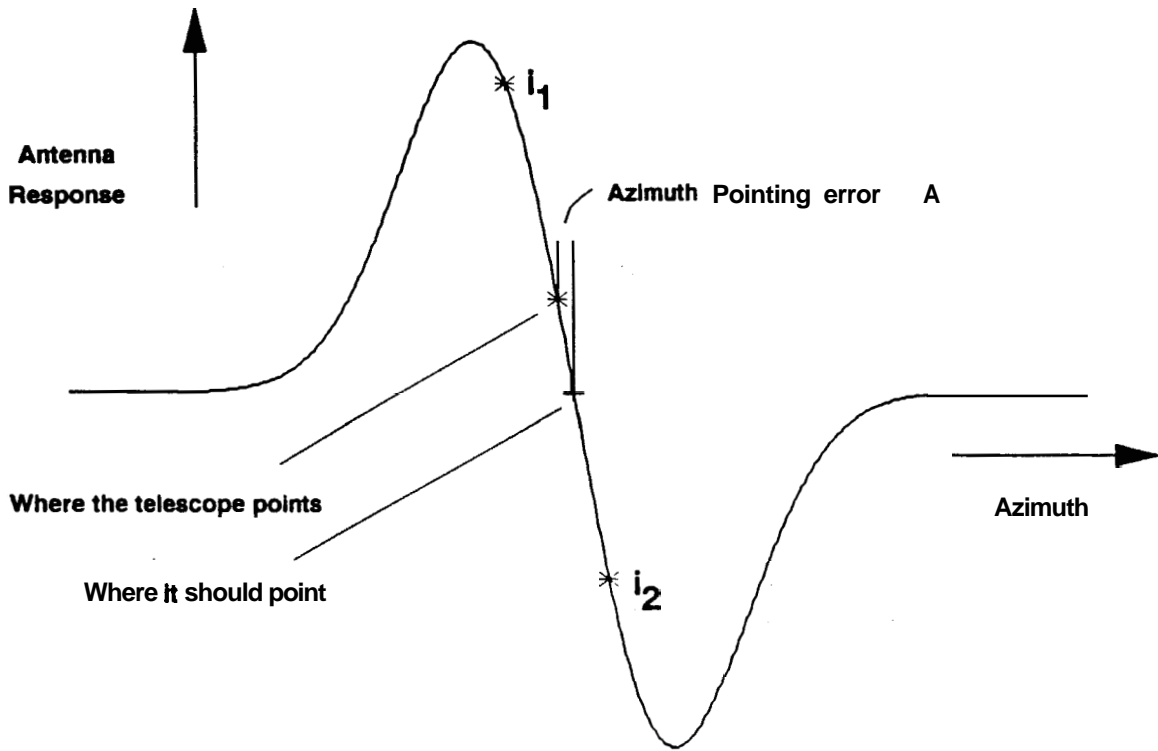


Figure 8: Beam-switched response as a function of azimuth and its use to obtain pointing-corrections.

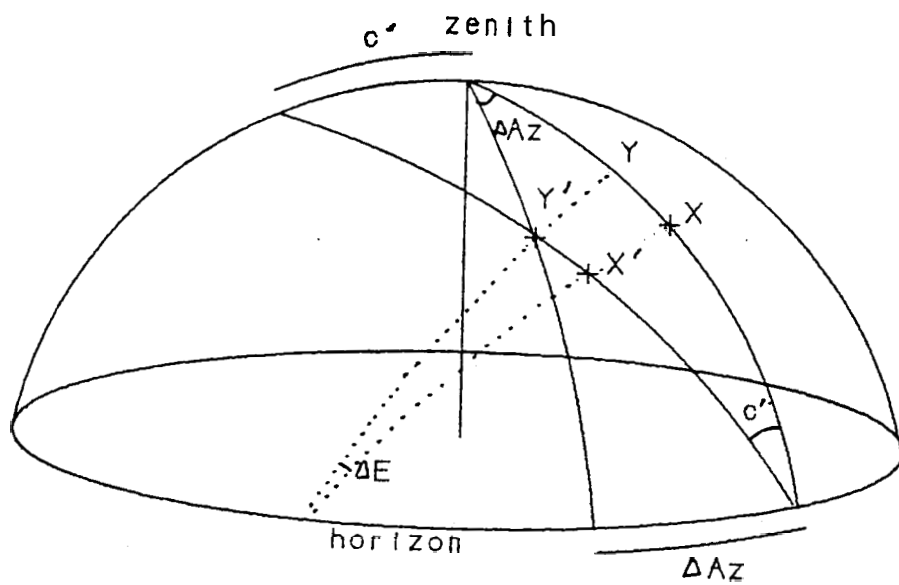


Figure 9: Pointing errors due to Elevation axis tilt

Azimuth offset due to a collimation error

Now

$$\sin \Delta A = \frac{\sin c}{\cos l} \quad (8)$$

therefore, to first order,

$$\Delta A = \frac{c}{\cos l} \quad (9)$$

Elevation offset due to collimation

(refer to Fig. 10.)

$$\Delta E = \arcsin \left(\frac{\sin l}{\cos c} \right) - l \quad (10)$$

which is negligible in the first order approximation.

Azimuth offset due to a tilt in the azimuth axis

$$\frac{\Delta A}{\tan E} = I \sin(A - A_t) \quad (11)$$

Elevation offset due to azimuth axis tilt

In Fig. 11, for small I , and to first order in ΔE

$$\Delta E = I \cos(A - A_t) \quad (12)$$

Finally, the azimuth and elevation offsets due to all these errors can be added together assuming that the effects of the errors act independently of each other. The maximum error in any of the mount parameters was found to be of the order of a hundred arc-seconds, so the use of first-order approximation remains valid.

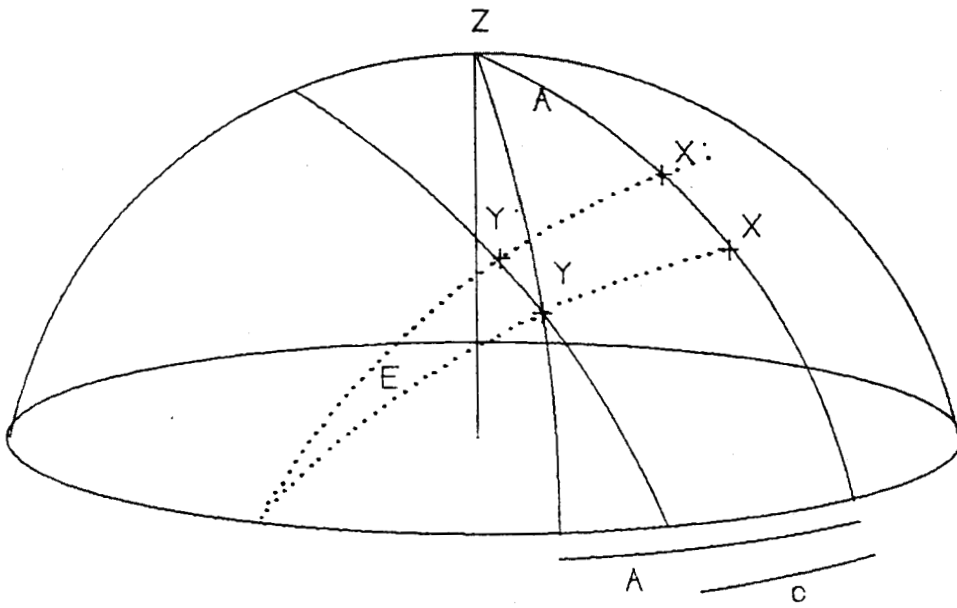


Figure 10: Pointing errors due to Collimation error

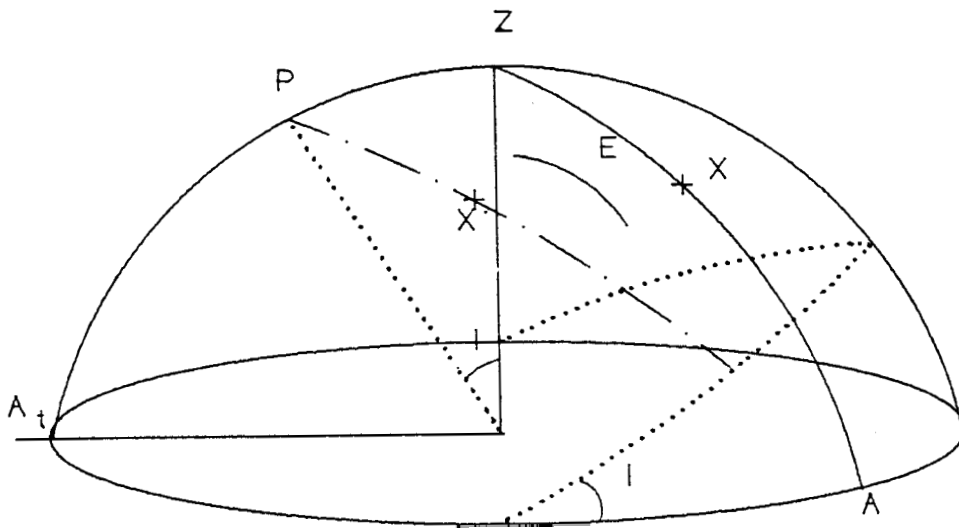


Figure 11: Pointing errors due to Azimuth axis tilt

The total offsets are given by:

$$\Delta A \cos E = A_o \cos E + c + c' \sin E + I \cos A_t \sin E \sin A - I \sin A_t \sin E \cos A \quad (13)$$

$$A E = E_o + B \cos E + I \cos A_t \cos A + I \sin A_t \sin A \quad (14)$$

Terms like $\sin(A - A_t)$ were expanded to obtain an expression that is linear in the parameter A_t so that a linear least-square fit program can be used.

2.3.2 Pointing offsets due to causes other than the mount errors

Clock error

The error in the local sidereal time amounts to an increase in the azimuth axis tilt in the east-west direction (in an algebraic sense). If the clock is faster, its effect is equivalent to an additional tilt of the azimuth axis towards west. Since the fitting program cannot separate this effect from the actual tilt in the azimuth axis, it was necessary to check the clock and correct it before making any observations. This was done by receiving the pulses transmitted at 10 and 15 MHz as a part of the time keeping service operated by the National Physical Laboratory, Delhi.

Receiver misalignments

The receiver misalignment will also contribute to pointing errors, corresponding to c , the collimation error in azimuth and AE , the elevation error, as defined earlier.

The receiver misalignment can occur in two ways. Firstly, the receiver axis **may** not be parallel to the telescope's optical axis. Secondly, the receiver may

be in a wrong position in the focal plane. We denote the horizontal and vertical components of this displacement by A_x and A_y , respectively. Then, in our Nasmyth focus system,

$$c = \Delta x \cos E + \Delta y \sin E \quad (15)$$

$$AE = \Delta x \sin E + A_y \cos E \quad (16)$$

e.g., A_x adds to the collimation error only when the telescope is pointing at the horizon. One could have added these terms to eqns (13) and (14) to fit for the pointing offsets, but we found it more reliable to minimize this misalignment in the hardware rather than allowing the least squares program to fit unreasonable values of parameters.

To achieve an alignment of all components of the receiver system to within 1mm, we used the following method which we call the compass method. Across a diameter of the elevation axis tube, a steel angle was clamped. A magnetic base was mounted on this angle to which a scribe was fixed. This scribe was pointed at the center of a part of the receiver e.g. the diplexer's center. The telescope was then moved in elevation from zenith to horizon. If the scribe's initial position was not collinear with the elevation axis, it inscribed a quadrant of a circle whose center gave the required point on the elevation axis where the part's center should lie. It was adjusted accordingly to be along the elevation axis. This procedure was iterated to reduce the radial lateral error in the placement of the feed, to the order of 0.5 to 1 mm. The elevation axis itself may be misaligned with respect to the horizontal plane or with respect to a plane normal to the possibly non-vertical azimuth axis. Therefore if the receiver system's optical axis is not collinear with the elevation axis then it would lead to elevation dependent errors as given by eqns (15) and (16). The advantage of our compass method described

above is that it directly defines the elevation axis which would have remained undetermined by any other method of alignment e.g., using a laser (Giordano 1989). Let x_0 and y_0 denote the center of the circle of radius r , a quadrant of which is inscribed on moving the telescope by 90° in elevation, then it is also the point of intersection of the elevation axis and the face of the device. Therefore the center of the device should be moved to this point. Let the initial and final co-ordinates of the scribe be $(0,0)$ and (x,y) , respectively, then

$$x_0 = \frac{(x + y)}{2}, y_0 = \frac{(y - x)}{2} \quad (17)$$

$$x_0 = \frac{(x - y)}{2}, y_0 = \frac{(x + y)}{2} \quad (18),$$

depending on which quadrant was traced. the final point of the scribe after the telescope has reached either zenith or horizon. These coordinates are measured directly on the face of the device to be aligned, using either a vernier or a scale. A misalignment of the tertiary is equivalent to that of the receiver except that there may be other side-effects like the beam throw may be such that the illumination is not symmetrical, or the beam-switching may not be purely in azimuth. Apart from these misalignments, an error in the position of the secondary (including tilts) will also lead to a collimation and a uniform elevation error. Because of the complicated dependence of the pointing errors on these misalignments, we have minimized the misalignments in all the components as far as possible, instead of trying to fit the pointing offsets to some complicated function of the misalignments.

Refraction

We have used Ulich's (1981) formula for refraction correction at mm wavelengths. This correction is applied on-line in the control program. The weather param-

eters are monitored and updated by the computer every ten minutes. We have found that the errors in the refraction correction are less than $\pm 3''$ for elevations down to 15° .

Sag function

The quadripod sag as measured at the centre of the secondary is about 1 to 2 mm when the telescope is looking at the horizon. This sag should give a maximum elevation error at the horizon, of about $50''$ and reduced by the cosine factor at higher elevations. But we found that the behaviour of elevation errors did not fit this simple cosine formula. We believe that the sag in the quadripod is accompanied by other effects like distortion of the primary dish, for example. Empirically, we found that the total error due to all these elevation dependent effects, can be modelled by a sine function of the elevation, whose amplitude, phase and period were found by a least-squares-fit.

$$AE = S_1 \sin(S_2 - S_3 \times el) \quad (19)$$

This term is added to the formula for elevation error given by eqn 14.

The following is the pointing model obtained during the 1989 season. The azimuth axis tilt was measured by inclinometers and the corresponding pointing corrections were applied according to

$$AA = (Y - Y_{mean}) \times \tan l \quad (20)$$

$$\Delta E = (X_{mean} - X), \quad (21)$$

where X and Y are the inclinometer readings and X_{mean} and Y_{mean} are their mean values, which were $14''$ and $-16''$, respectively. The remaining parameters were as follows:

Azimuth DC error	100"
Collimation error in azimuth	-8"
Tilt in elevation axis	0"
Collimation error in elevation (DC error)	383"
Sag parameters: S1	25"
S2	3.28 radians
S3	2.79 radians

Figs. 12–14 show the residuals measured on Jupiter, after using the above pointing model in the control program.

2.4 Measurements of Aperture Efficiency

Calculation of Aperture efficiency

For a point source of flux density S , the effective area A , of the telescope is given by

$$SA = 2kT_m \quad (22)$$

where T_m is the measured antenna temperature corrected for the atmospheric attenuation. Here k , is Boltzmann's constant. The aperture efficiency is given by

$$\eta_A = A_e/A_p \quad (23)$$

where A_p is the physical area of the dish. If the source is not a point source but a disc of radius R , then we have to correct T_m by a factor which can be calculated as follows: Let a point source of unit flux density be observed on the peak of a gaussian beam of unit amplitude. If we spread this source into a disc of radius R , with energy density $1/\pi R^2$, see Fig. 15, where $r_{\frac{1}{2}} = \sigma\sqrt{\ln 2}$, then the energy measured by the beam is given by

$$c = \frac{1}{\pi R^2} \int_0^R \exp^{-r^2/\sigma^2} 2\pi r dr \quad (24)$$

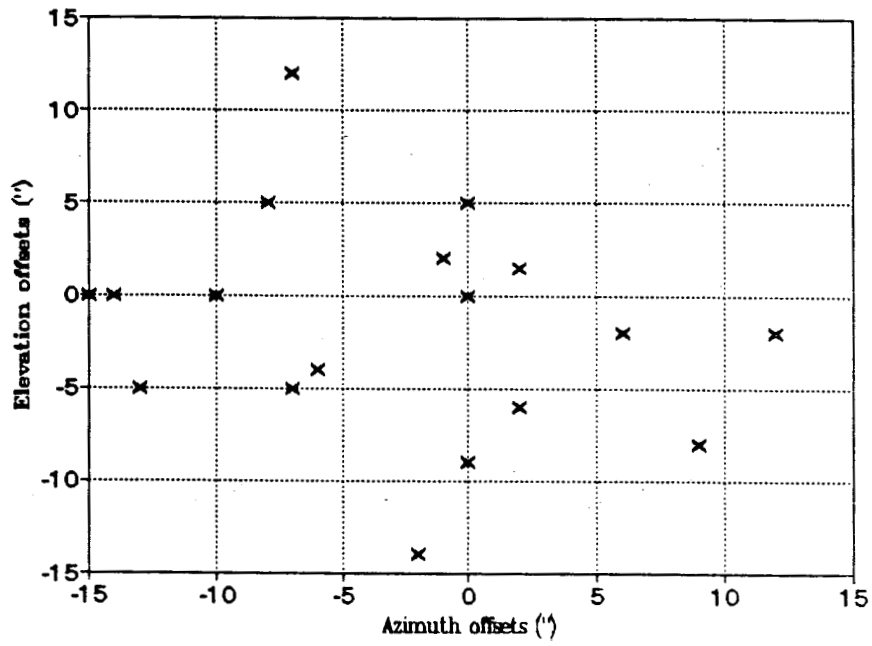


Figure 12: Residual pointing errors on Jupiter (1989): Elevation offsets versus Azimuth offsets

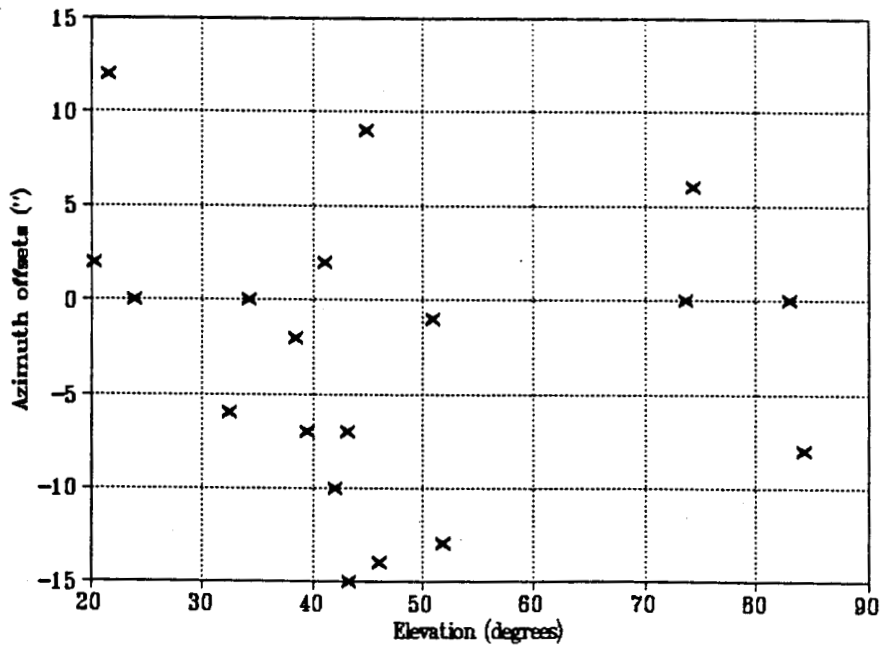


Figure 13: Azimuth offsets versus Elevation

$$= \frac{(1 - \exp(-X))}{X} \quad (25)$$

where $X = \left(\frac{R\sqrt{\ln 2}}{r_{\frac{1}{2}}} \right)^2$. Because of this ‘spreading’ of the point source, we now find the antenna temperature to be $c \times T$ instead of T . Thus, to use the point source formula, we have to divide the measured value of the antenna temperature by the correction factor c .

$$\frac{T_m}{c} = \frac{A_p \eta_A S}{2k} \quad (26)$$

$$= \frac{A_p \eta_A T_B \Omega}{\lambda^2} \quad (27)$$

where Ω is the solid angle subtended by the planet at the time of measurement.

Thus

$$\eta_A = \frac{T_m}{c} \frac{\lambda^2}{\Omega T_B A_p} \quad (28)$$

$$= 0.0496 \frac{T_m}{c} \left(\frac{170}{T_B} \right) \left(\frac{30}{a} \right)^2 \left(\frac{87}{\nu} \right)^2 \quad (29)$$

where T_B is the planet’s brightness temperature, a is its diameter in arc seconds and ν is the frequency in GHz.

The aperture efficiency **was** calculated from continuum scans taken on Jupiter and Venus. These are elevation scans with beam-switching in azimuth in the 0—18 mode, i.e., ON: full illumination of the secondary and OFF: almost missing the secondary. Figures 16 & 17 show some typical scans. The negative shift in the baseline comes due to a difference in the amount of ambient temperature picked up from OFF and ON beams respectively. We have measured the antenna temperature by fitting to the scan a gaussian whose peak value is measured from the baseline. The program CHART is used to acquire the scan and ELSCAN fits the gaussian. ELSCAN also calibrates the scan by using the values of the synchronous detector voltage values from the chopper wheel, which are recorded

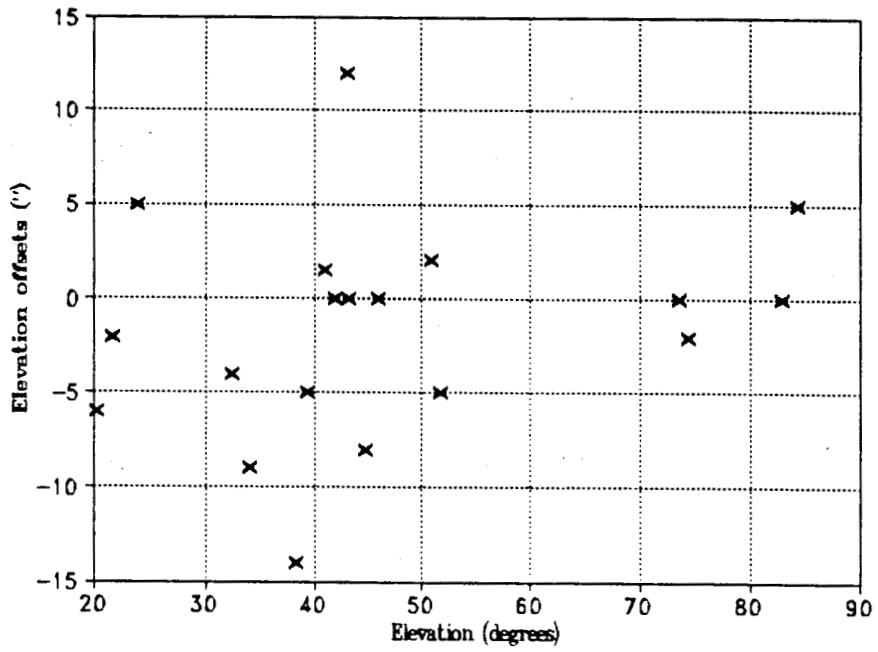


Figure 14: Elevation offsets versus Elevation

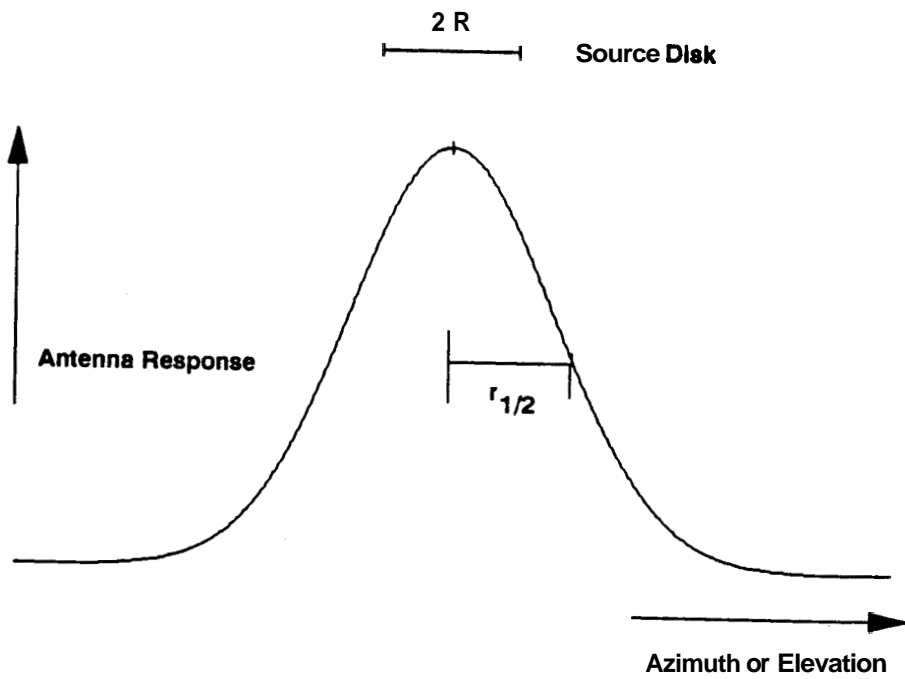


Figure 15: Gaussian main-beam and Planet's disc

before and after the scan.

We have measured the aperture efficiency at three frequencies, 87.7, 96.6 and 113.8 GHz. The results are presented in Table 3.2 (p77) in the following chapter on calibration errors. Fig. 18 is a plot of the efficiency due to surface errors as given by the Ruze formula

$$\eta_A = \eta_0 \exp \frac{-4\pi\epsilon^2}{\lambda}. \quad (30)$$

In this figure, the measured values are at 87, 97, 108 and 113 GHz. The efficiency is normalized to the value at 87 GHz. Except for the efficiency at 113 GHz, we see that the r.m.s. surface error indicated by these measurements lies between 120 to 140 μ .

2.5 Measurement of Beam Efficiency

The quantity that is most often quoted in literature as "beam efficiency", is usually the extended source efficiency η_s , as defined by Kutner and Ulich (1981). This is obtained by comparing the antenna temperature on the Moon with its brightness temperature. Observing the full-moon, we have obtained $\eta_s = 0.85$. With this method, one measures the amount of power in the response pattern of the antenna within the Moon's solid angle. If the antenna has substantial amount of power in its error lobes, which may be much larger than the main lobe but still within the solid angle of the Moon, then η_s may approach unity, while having a poor main beam efficiency which remains undetermined. In our telescope this situation can arise from panel-to-panel deformations. Taking 1.2m as the diameter of a panel, at the wavelength of 2.6mm, the size of the error beam due to these deformations is of the order of 450". A much larger error

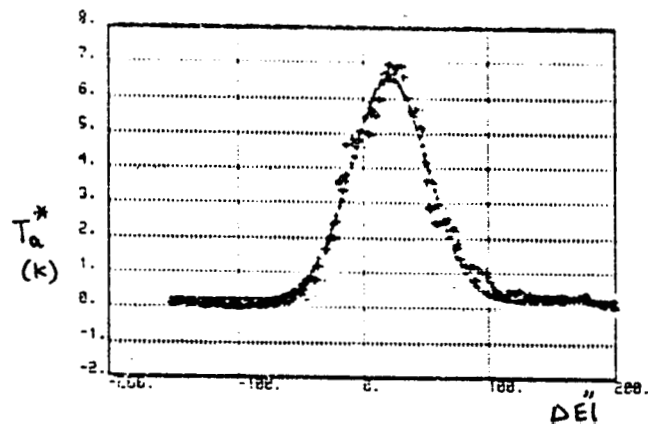
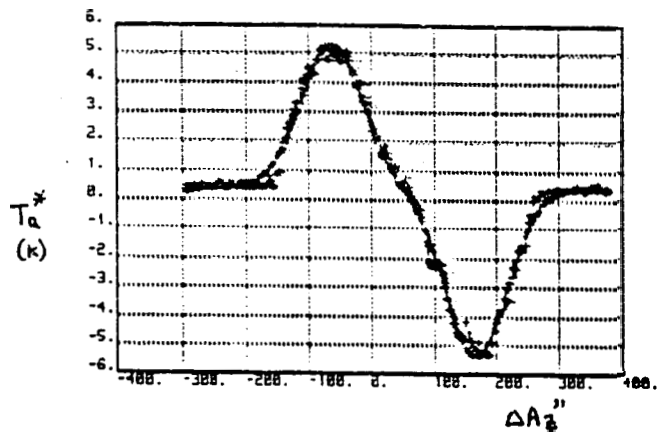


Figure 16: Beam-switched scans on Jupiter with fitted curves

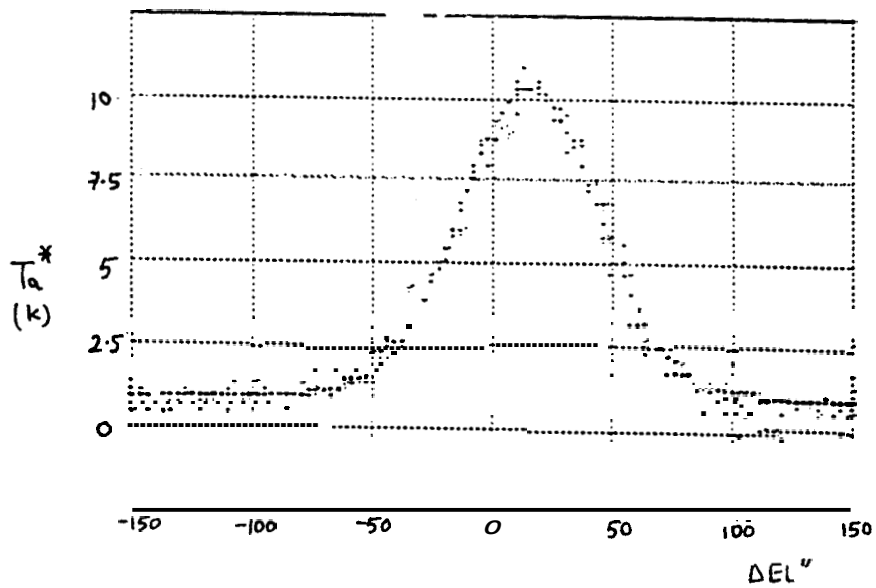


Figure 17: Elevation scan on Jupiter

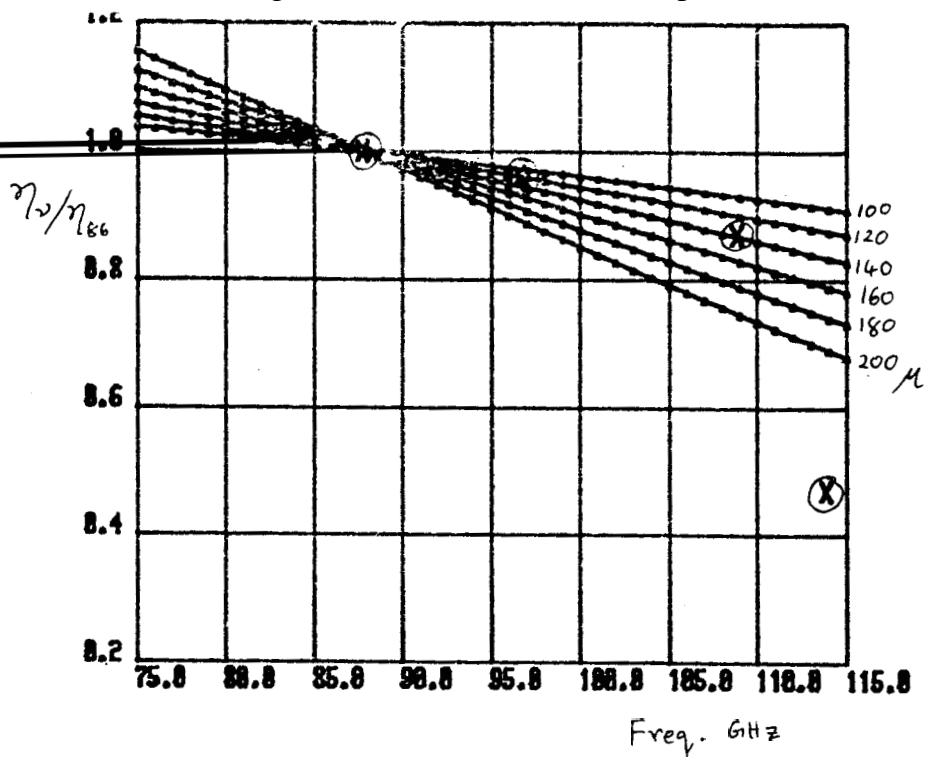


Figure 18: Decrease in Aperture efficiency due to surface errors

beam can arise due to the forward spillover scattering past the secondary, though this part of the error beam is expected to be much weaker.

We have measured the forward main beam efficiency by taking a continuum scan of the Sun. In the following section, we present the method and results. We also summarize the definitions of various efficiencies as defined in the paper by Kutner and Ulich (1981).

A continuum scan of the Sun is shown in Fig. 19. The total power voltage is plotted against arc-seconds offset in elevation from the centre of the Sun. The half-power points occur at $\pm 1000''$ giving the radius of the Sun to be $1000''$ at 115 GHz. This result (see Fig. 20) is independent of the size of our main beam as long as it is assumed to be symmetrical, and the brightness distribution of Sun is described by a disc. On the scan, points a and b indicate the offsets where the voltage starts deviating from the baseline as the Sun enters the error beam. This occurs at $2850''$, from which we get the radius of the error pattern to be $1850''$ (see Fig. 21).

We have measured the main lobe beam size to be about $60''$ (FWHM) on Jupiter. Assuming the null points to be $60''$ away from the centre, we find that the Sun's limb begins to enter the main lobe at an offset of $1060''$ where the signal corresponds to 0.3 volts from the baseline. This value represents the overlap of the error pattern with the Sun as shown in Fig. 22.

The forward beam efficiency is the ratio of the response within the main lobe to that within the (error pattern + main lobe). We assume that the error pattern is constant with respect to both polar and azimuthal angles (it is a disc). With these assumptions we can estimate the response within the total error pattern by scaling up the 0.3 volts by a factor which is the ratio of the

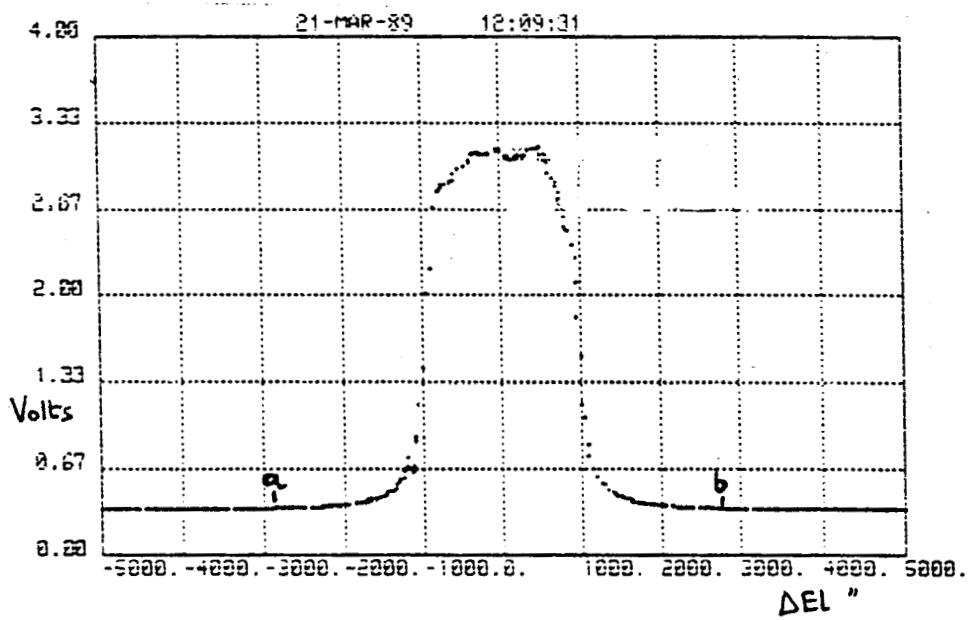


Figure 19: Continuum (total-power) scan on the Sun

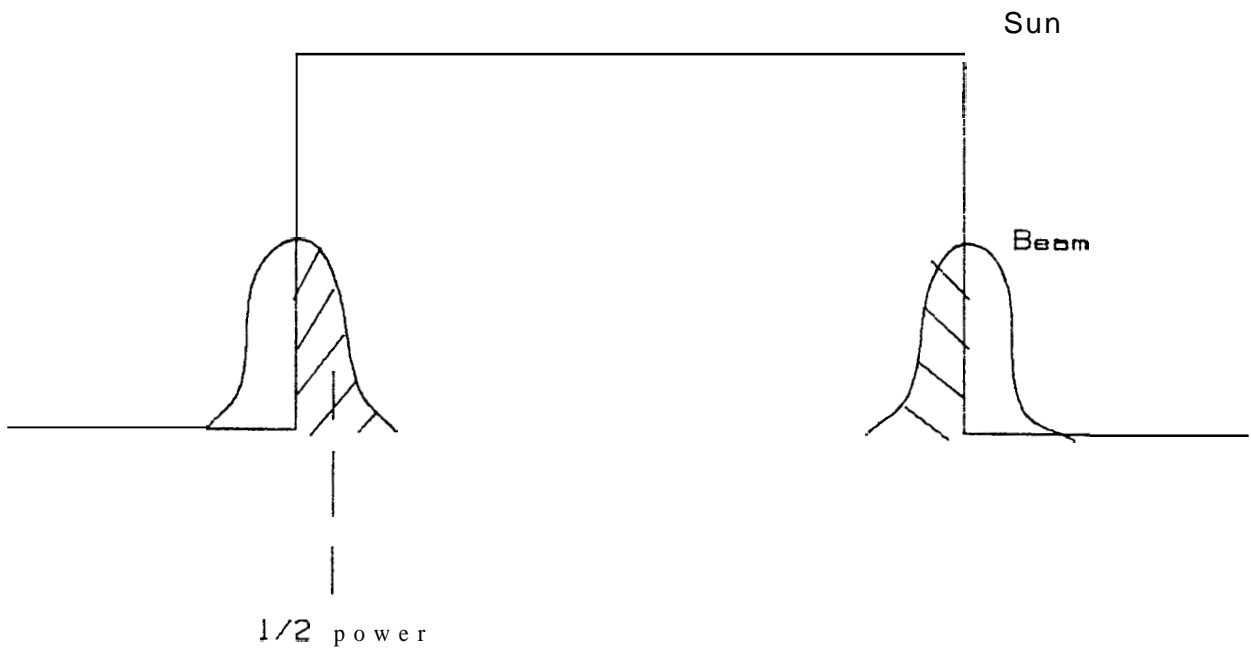


Figure 20: Figure explaining why Half-power points give the measurement of diameter regardless of the size of the beam

total error pattern and the error pattern covered by the Sun, i.e.,

$$\begin{aligned} V_{error} &= 0.3\text{volts} \times \pi (R_{error}^2 - R_{FWHM}^2) / A \\ &= 1.61\text{volts} \end{aligned} \quad (31)$$

where $R_{FWHM} \approx 30''$ and A is the overlap area derived as shown later.

When the telescope is pointing at the centre of the Sun (Fig. 23), we get 2.83 volts from the baseline. Subtracting the error lobe pattern contribution from this (assuming it to be uniform) we get 2.53 volts. The forward beam efficiency is then given by

$$\eta_{fs} = \frac{\text{main beam contribution}}{(\text{main beam} + \text{error beam}) \text{ contribution}} \quad (32)$$

using the measured values, this amounts to 0.61. This is the first estimate of the forward beam efficiency of the 10.4m Telescope, at the frequency of 113.8 GHz.

The overlap area used in the above calculation is derived as follows:

case 1: see Fig. 23.

$$A = \frac{r^2}{2}(\alpha - \sin \alpha) + \frac{R^2}{2}(\beta - \sin \beta) \quad (33)$$

where

$$\cos \alpha/2 = \frac{D^2 + r^2 - R^2}{2Dr} \quad (34)$$

$$\cos \beta/2 = \frac{D^2 + R^2 - r^2}{2DR} \quad (35)$$

case 2: see Fig. 24. The area of sector ABC is given by

$$\frac{R^2}{2}(\beta - \sin \beta) \quad (36)$$

where the above equation for $\cos \beta/2$ still holds. The area of ABE is given by

$$A = \pi r^2 - (\text{area of } ABC') \quad (37)$$

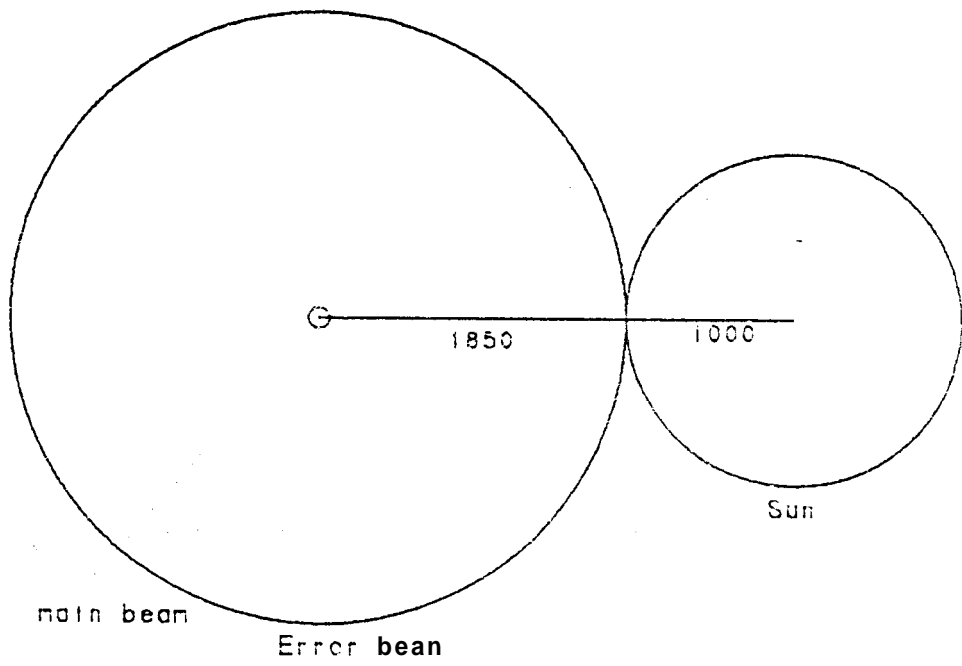


Figure 21: Error pattern about to enter the disc of the Sun

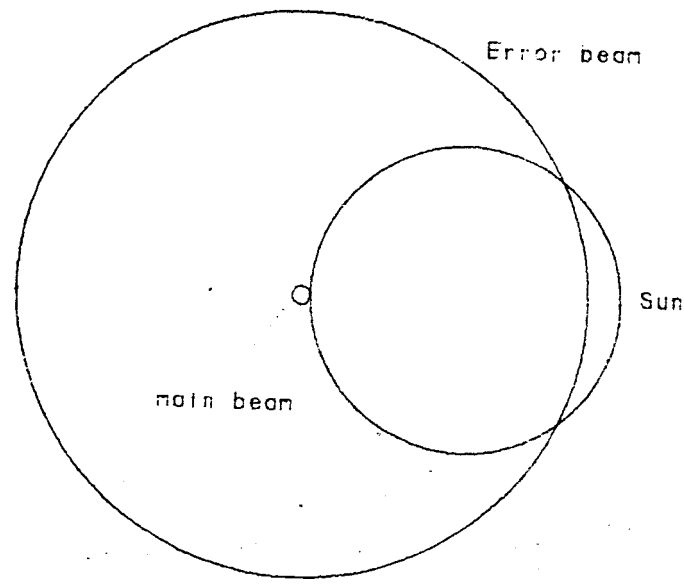


Figure 22: Main-lobe about to enter the disc of the Sun

$$= \pi r^2 - \frac{r^2}{2}(\alpha' - \sin \alpha') \quad (38)$$

$$\frac{\alpha'}{2} + \frac{\alpha}{2} = \pi \quad (39)$$

therefore

$$\alpha' = 2 \left(\pi - \cos^{-1} \left(\frac{D^2 + r^2 - R^2}{2Dr} \right) \right) \quad (40)$$

and

$$A = \frac{R^2}{2}(\beta - \sin \beta) + \pi r^2 - \frac{r^2}{2}(\alpha' - \sin \alpha') \quad (41)$$

Note that cases 1 and 2 are not relevant when $(D + r) < R$, i.e., when the Sun is within the error circle. (Then, the overlap area is simply the area of the Sun's disc).

Summary of the definitions of various efficiencies (Kutner and Ulich,1981).

The measured antenna temperature (neglecting ohmic losses and atmospheric attenuation) is related to the brightness temperature of the source by

$$kT_A = \frac{1}{2} \frac{2kT_B}{\lambda^2} A_e \int_{4\pi} (B \times P) d\Omega \quad (42)$$

where B is the normalized angular distribution of intensity, and P is the antenna response pattern. The effective beam of the antenna is given by

$$\Omega_A = \int_{4\pi} P d\Omega. \quad (43)$$

Since $A_e \Omega_A = X^2$,

$$T_A = T_B \times \frac{\int_{\Omega_{source}} (B \times P) d\Omega}{\int_{4\pi} P d\Omega} \quad (44)$$

Which can be written as,

$$T_A = T_B \times \frac{\int_{source} (B \times P) d\Omega}{\int_{mainbeam} P d\Omega} \times \frac{\int_{mainbeam} P d\Omega}{\int_{4\pi} P d\Omega}, \quad (45)$$

where the first ratio of integrals on the right hand side, is called the source coupling factor and the second one is called the main beam efficiency. Kutner and

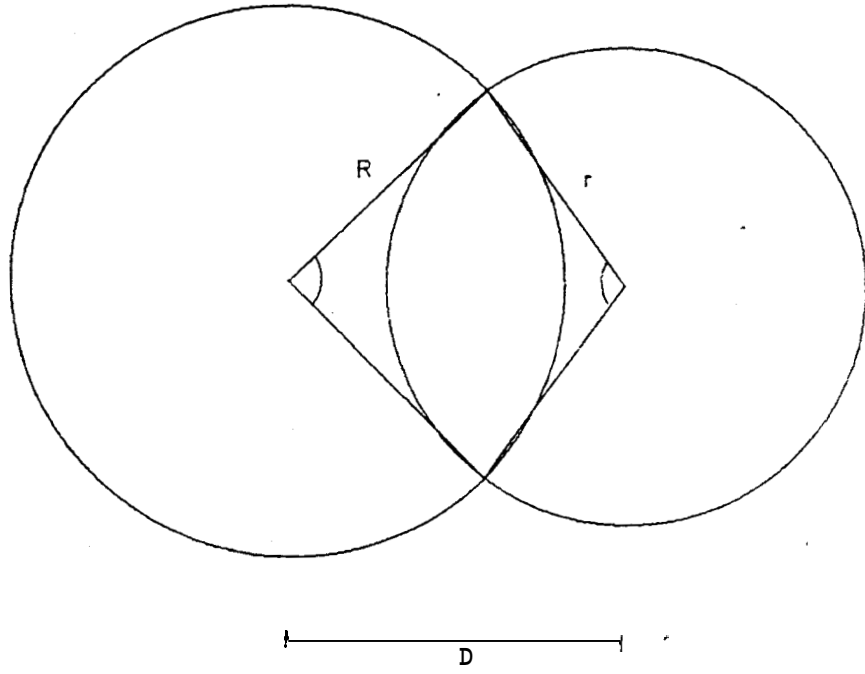


Figure 23: Case 1.

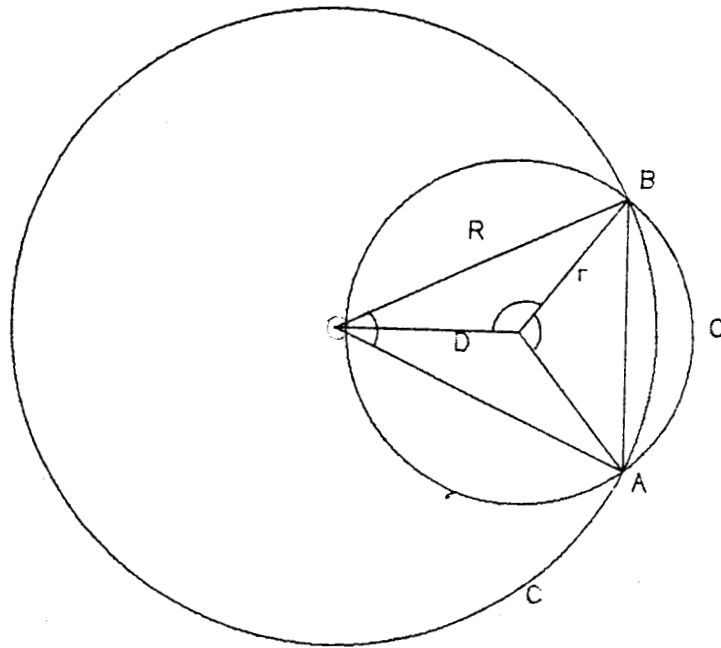


Figure 24: Case 2.

Ulich define $T_R^* = \eta_c T_B$ (and recommend its use in reporting observations). T_R^* is corrected for everything except the coupling of the antenna's diffraction pattern to the source. However, the observations reported here are all of effectively point sources and therefore this distinction between T_R^* and T_A^* is not necessary.

The main beam efficiency can be further split up into

$$\frac{\int_{\text{main}} P d\Omega}{\int_{2\pi} P d\Omega} \times \frac{\int_{2\pi} P d\Omega}{\int_{4\pi} P d\Omega} \quad (46)$$

Here, the first term is called the 'forward spillover scattering efficiency', η_{fss} , and the second term is called the 'rear spillover scattering efficiency', η_{rss} .

The motivation for these definitions is twofold: 1. In a cassegrain telescope a small part of the feed's response may spillover around the secondary, leading to $\eta_{fss} \neq 1$. 2. In chopper wheel calibration the rear spillover scattering gets cancelled out but the T_A^* remains uncorrected for η_{fss} .

Kutner and Ulich define the extended source efficiency as

$$\eta_s = \eta_c \eta_{fss} \eta_{rss} \eta_r \quad (47)$$

where η_r denotes the ohmic losses. $\eta_r \eta_{rss}$ is the same as η_l of Ulich and Haas (1976) i.e., the quantity,

$$(1 - \eta_l) \times T_{\text{ambient}} \quad (47)$$

gives the T_{stray} , (y-intercept on the sky-dip plot).

The extended source efficiency η_s can be measured on the Moon but one has to be cautious if the error pattern is comparable or larger than the Moon (as with our telescope). If η_s can be reliably estimated, then η_{fss} is given by

$$\eta_{fss} = \frac{\eta_s}{\eta_l} \quad (48)$$

where η_l is measured from the dip plot. From a Moon-scan measured on April 6, 1989, we have obtained a value of $\eta_s \approx 0.6$. The Dip-measurements on sky usually give a value for $T_{stray} \approx 20K$, which implies an η_l of about 0.9. Thus, within an error of about 10%, we find that the value of η_{fss} obtained this way, is in agreement with the value estimated from the Sun-scan.

A widely used technique is to model the main lobe as a gaussian. Then by using its width and the measured value of η_A , one can obtain the beam efficiency as well. In our case this method yields a value of beam efficiency to be 0.54, while the above analysis (p55) gave 0.61. This indicates that the main beam **shape** can be well approximated by a gaussian.

REFERENCES

- Christiansen W. N., Hogbom J. A., 1969, *Radio Telescopes* 1st Ed., Cambridge Univ. Press, p 72.
- Giordano P., 1989, *ESO Messenger* No. 57, p 65.(SEST annual report).
- Kutner M. L., Ulich B. L., 1981, *Ap. J.* 250, 341.
- Leighton R. B., 1978, 'A 10m telescope for mm and sub-mm Astronomy', California Institute of Technology, Report — May 1978.
- Maiyah U.N. 1983, Ph.D. Thesis, University of Mysore.
- Ulich B. L., 1981, *Int. Journal of IR and MMW*, 2, 293.
- Ulich B. L., Haas R. W., 1976, *Ap. J. Suppl. Ser.* 30, 247.
- Williams D. R. W., 1976, *Methods of Experimental Physics*, (Ed. Meeks M. L.) 12 c, p 31.